

On a possibility of earthquake forecast by radio observations in the VHF band

Yoshio Kushida* and Reiki Kushida*
International Frontier Program on Earthquake Research

Anomalous time variation of the intensity of radio waves from radio stations beyond the line of sight was studied in the VHF band for the period August 1995 to July 1997. Significant anomalies were observed preceding large earthquakes and they were applied for the forecasting of earthquakes. Methods to forecast the date, the magnitude and the focus location of future earthquakes are described and a model to explain the mechanism of the correlation between the anomalies and earthquakes is discussed.

Introduction

In 1993, we started the meteor counting by observing the radio echoes in the very-high-frequency (VHF) band using a commercially provided FM receiver set. Radio echo is observed as a pulsed delivery of radio waves from a radio station located beyond the line of sight, which typically continues for hundreds of milliseconds. The radio waves are delivered by specular reflection on plasma tubes generated in the ionosphere on the passage of meteors through the atmosphere.¹⁾

We recorded the time variation of radio wave intensity using a chart recorder. Radio echoes were recorded as sharp spikes on a baseline. We sometimes observed an anomalous behavior of the baseline. By the end of 1994, we empirically recognized that such an anomalous behavior appeared a few days before the earthquakes occurred between our observatory and the radio station tuned by the receiver set. We, however, did not pay enough attention to the possible correlations between earthquakes and anomalies in radio observation until the Hyogo-Nanbu Earthquake (M7.2) occurred on 17 January 1995. The detection of radio echoes became difficult due to extraordinary baseline fluctuations, which reached its maximum value on the night of 14 January 1995.²⁾ The baseline fluctuation gradually returned to the usual level about 20 days after the earthquake. We learned that such extraordinary anomalies were also observed by amateur astronomers and that civilians in the seismic region experienced large noises in receiving radio programs, which motivated us to extend our radio observation. After we carried out preliminary observations during February to April 1995, we increased the number of receiver sets and initiated continuous monitoring of baseline behavior to study a possibility of earthquake forecasting using radio observation in the VHF band.

In the present paper, we describe our method of earthquake forecast based on radio observations in the period from 24

July 1995 to 31 July 1997. All the dates and times are described in terms of Japan Standard Time.

Observation system and types of anomalies

Our receiver system is schematically shown in Fig. 1. A 5-element Yagi antenna (MASPRO FM-5E) is directed vertically and the normal vector of the antenna plane is directed with an offset angle θ towards an FM radio station located beyond the line of sight. Our observatory is located at N35°52'45", E138°22'04" and 1055 m above sea level and the range of sight is about 200 km. Table 1 shows the radio frequencies, the output powers and the locations of FM radio stations used in our observation.

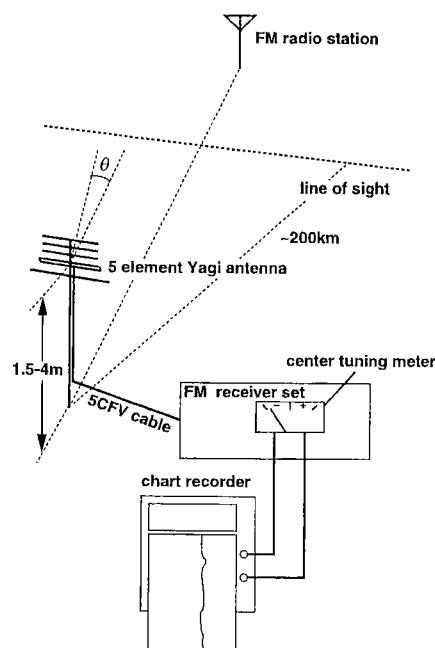


Fig. 1. A schematic view of the observation system. A 5-element Yagi antenna (MASPRO FM-5E) is connected to a commercially available FM receiver set with a 5CFV cable. The FM receiver set is equipped with a center tuning meter and the voltage of the center tuning meter is recorded by a chart recorder.

The antenna is connected with a 5CFV cable to a commercially provided FM receiver set equipped with a center tuning meter. The FM receiver set is tuned slightly offset to the frequency of the FM radio station and the voltage level of the center tuning meter is recorded by an analog chart recorder.³⁾

* Permanent address: Yatsugatake South Base Observatory, kushida@proteus.riken.go.jp.

Table 1. Frequencies and output powers of FM radio stations used in our observation up to July 1997. (a) The exact location of the radio station tuned by the receiver H is not known to us. We assume that the radio station is located in the vicinity of Naha city of Okinawa Island.

receiver	f_0 [MHz]	P [kW]	location of radio station	observation period	receiver set	chart recorder
A	89.1	1.0	N44°57' E142°09'	1997/4-	Victor JT-V45	National VP6567A
B	80.4	5.0	N43°04' E141°12'	1996/5-	Pioneer TX7600	Yokogawa 3047
C	77.5	1.0	N37°42' E138°49'	1995/3-	Pioneer TX7600	National VP6567A
D	77.1	5.0	N38°14' E140°52'	1993/8-1995/2 1995/3-1995/6 1995/6-1995/8 1995/8-1996/9 1996/9-1997/1 1997/1-	Pioneer TX7600 Pioneer TX7600 Trio KT5500 Trio KT5500 Sansui TU1100 Sansui TU1100	National VP6710A National VP6567A GRAPHTEC SR6511 National VP6567A National VP6567A Yokogawa 3057
E	77.8	10.0	N35°09' E136°58'	1993/8-	Pioneer TX7700	National VP6567A
F	89.4	1.0	N34°58' E135°38'	1995/3-1997/1 1997/1-	Trio KT5300 Trio KT5300	GRAPHTEC SR6511 Yokogawa 3057
G	89.1	6.0	Okinawa ^(a)	1996/7-1997/1 1997/1-	Pioneer F005 Pioneer F005	National VP6567A Yokogawa 3057
H	87.3	1.0	N26°13' E127°44'	1996/7-1997/1 1997/1-	Sansui TU1100 Sansui TU1100	National VP6567A Yokogawa 3057

The model numbers of FM receiver sets and chart recorders are shown in Table 1.

The center tuning meter outputs the voltage which is proportional to the difference between the tuned frequency and the input frequency as shown in Fig. 2. The output voltage depends also on the input level for the case where the input radio wave is very weak. Therefore, the center tuning meter functions as a sensitive intensity meter for weak radio waves for the case where the receiver set is tuned with an appropriate frequency offset. Each frequency offset is empirically adjusted so that each system becomes most sensitive to anomalies described below. Offset values are in the range of 70–150 kHz.

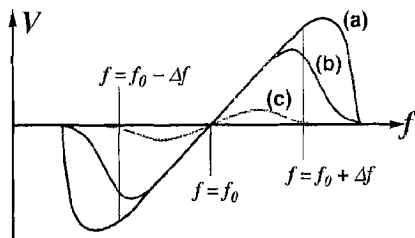


Fig. 2. A schematic illustration of the output voltage of the center tuning meter as a function of the input frequency. The output voltage is proportional to the difference between the tuned frequency and the input radio wave frequency. The curve changes its shape depending on input power. The curve (a) is the response for an ordinary radio power, (b) for a weak radio power and (c) for a very weak radio power. If the receiver set is tuned with an appropriate frequency offset, the center tuning meter functions as a sensitive radio wave intensity meter. The frequency offset is adjusted in the range of 70–150 kHz during the observation.

An example of the chart recording of the receiver D obtained before daybreak of 11 September 1995 is shown in Fig. 3. Radio echoes were recorded as sharp spikes together with the reflections caused by aircraft, and are seen to exceed the noise level. The noise causes an oscillation of the chart recorder pen with a frequency of 2–3 Hz, which results in thickening

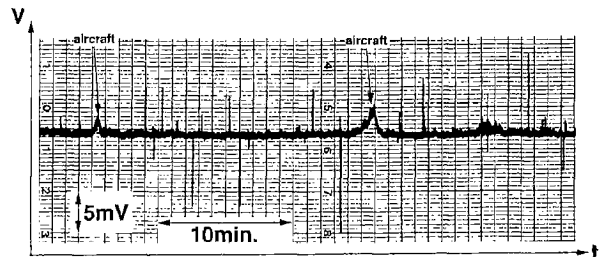


Fig. 3. An example of radio echoes due to meteors and reflections by aircraft recorded by the receiver D before daybreak on 11 September 1995. The pulse widths of meteor radio echoes are less than a second, while aircraft reflections are of the order of a minute.

of the baseline. The time duration of the aircraft signals are of the order of a minute. Aircraft signals can be identified from the time duration and also by comparing two or more receiver charts since they are detected by different receivers simultaneously.

Figure 4 depicts an example of an anomalous behavior accompanied by a sporadic E, observed on 2 January 1998 by the receiver A. Sporadic E signals usually last for about 30 to 120 minutes. Radio signals due to sporadic E can be demodulated as well as the case of meteor radio echoes. The effect of sporadic E can be unambiguously identified because most receivers show extraordinarily large baseline fluctuations with a time duration of the order of an hour.

After removing the signals due to meteor radio echoes, aircraft and sporadic E, there still remain significant time variations in the baseline. Possible effects caused by thunder clouds are also removed by taking into account the on-line weather information which is commercially available.⁴⁾ The remaining time variations which exceed the noise level are referred to as anomalies. The baseline thickness corresponding only to the noise level is referred to as the usual baseline thickness. The voltage value corresponding to the usual baseline thickness is denoted by v_0 .

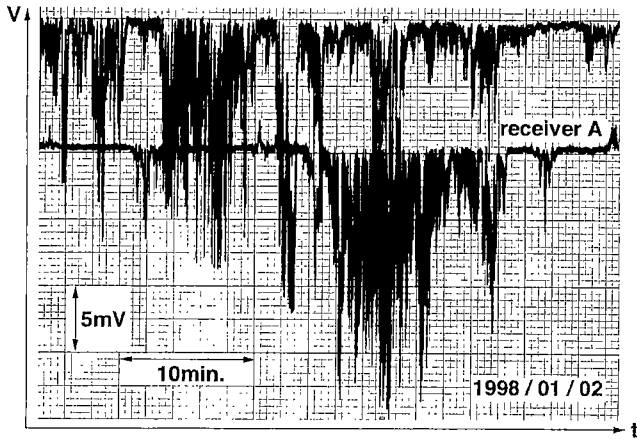


Fig. 4. An example of an anomalous behavior of the baseline due to a sporadic E recorded by the receiver A on 2 January 1998. Radio echoes are not identified because of the extremely large baseline fluctuation. The upper chart was recorded by a test receiver.

Most anomalies can be categorized into four types as shown in Fig. 5. The first type shows the time evolution of voltage which can be approximated by a function of the form $V(t) = V_0 + \Delta V(1 - \exp(-(t - t_0)/\tau))$. This type of anomaly is referred to as charge-discharge anomaly (CD-anomaly) in an analogy with the time evolution of voltage during charging and discharging of a capacitor. The CD-anomaly is characterized by the time constant τ and the amplitude ΔV . The time

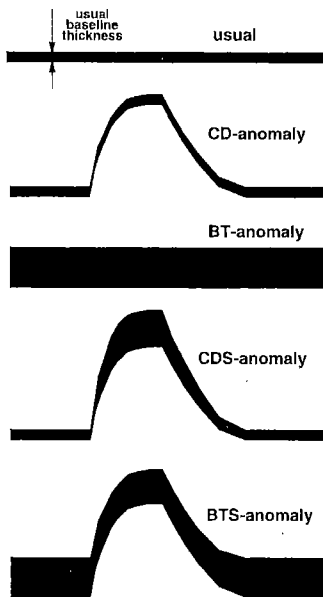


Fig. 5. Four types of anomalies are schematically illustrated. CD-anomaly is the time variation of the baseline exceeding the usual baseline thickness, which is similar to the time evolution of the voltage of a capacitor in a charge-discharge process. BT-anomaly is observed as the increase of the baseline thickness. The third type is a CD-anomaly accompanied by a BT-anomaly referred to as a CDS-anomaly. An increase in line thickness is observed during the CD-anomaly, while it is at the level of the usual baseline thickness out of the CD-anomaly. The fourth type is a BT-anomaly accompanied by a CD-anomaly referred to as a BTS-anomaly. The line thickness is enhanced regardless of the existence of CD-anomaly.

constant τ ranges between 1 to 10 minutes. The significance of the CD-anomaly is measured by the ratio

$$\xi = \frac{\Delta V}{v_0}, \quad (1)$$

where v_0 is the usual baseline thickness. CD-anomalies with a significance of $\xi < 1$ are ignored.

The second type of anomaly is the increase in the baseline thickness. This type of anomaly is referred to as baseline-thickness anomaly (BT-anomaly). The increase in baseline thickness is caused by an oscillation with a frequency of a few Hz. The significance of BT-anomaly is measured by the enhancement factor of baseline thickness defined as

$$\eta = \frac{v}{v_0}, \quad (2)$$

where v is the voltage value corresponding to the baseline thickness in a BT-anomaly.

The third type is a CD-anomaly accompanied by a BT-anomaly. An increase in line thickness is observed during the CD-anomaly, while the thickness is at the level of the usual baseline thickness out of the CD-anomaly. This type of anomaly is referred to as a CD-dominant superposed anomaly (CDS-anomaly). A CDS-anomaly can be decomposed into a CD-component and a BT-component. The significance of the CDS-anomaly is measured by the values ξ and η of corresponding components. The CDS-anomaly is also characterized by the time constant τ of its CD-component. We note that the line thickness is not increased in the case of a simple CD-anomaly.

The fourth type is a BT-anomaly accompanied by a CD-anomaly. The line thickness is enhanced irrespective of the existence of the CD-anomaly. This type of anomaly is referred to as the BT-dominant superposed anomaly (BTS-anomaly). The significance of the BTS-anomaly is measured by the val-

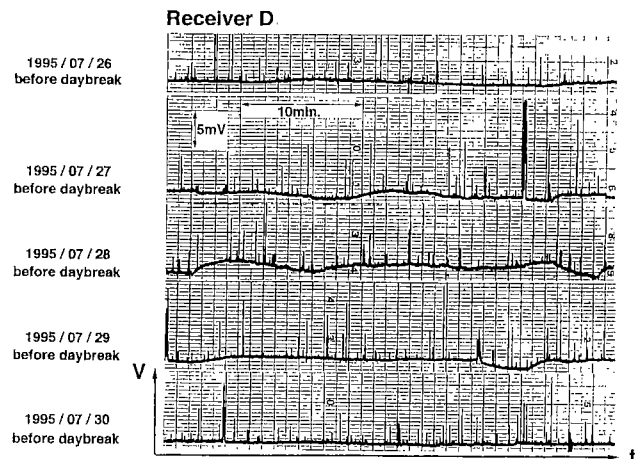


Fig. 6. Example of a charge-discharge anomaly recorded by the receiver D. Typical parts of the charts recorded from 26 July 1995 to 30 July 1995 are shown. Significant CD-anomalies first appeared on 27 July 1995 and continued up to 29 July 1995. The anomaly strength attained its maximal value on 28 July 1995. Earthquake {1} occurred on 30 July 1995 in the CD-sensitive region of the receiver D.

ues ξ and η corresponding CD- and BT-components. The BTS-anomaly is also characterized by the time constant τ of its CD-component.

Anomalies which cannot be categorized into the above four types are referred to as exceptional anomalies.

Figure 6 depicts an example of the CD-anomaly, which was observed with the receiver D during the period from 26 July 1995 to 30 July 1995. The baselines have significant time variations which can be approximated by the charge-discharge function, and the line thickness is not enhanced during the CD-anomaly.

Figure 7 depicts the example of a BT-anomaly, which was observed with the receivers G and H during the period from 17 October 1996 to 20 October 1996. BT-anomalies were

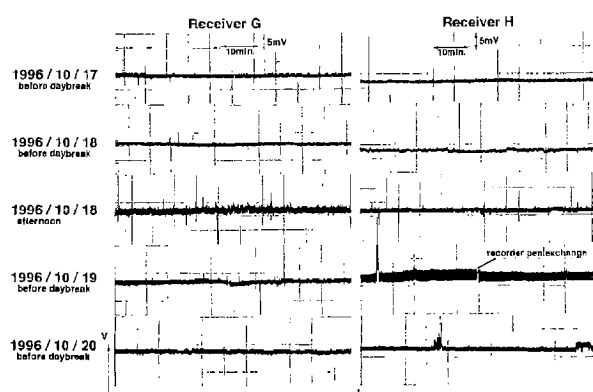


Fig. 7. An example of the baseline-thickness anomaly recorded by the receivers G and H. Typical parts of the charts recorded from 17 October 1996 through 20 October 1996 are extracted and shown in the figure. Weak BTS-anomalies are also seen among the BT-anomalies. Receiver G showed a maximal value on 18 October 1996 and receiver H on 19 October 1996. In the close vicinities of CD-sensitive regions of receivers G and H, earthquakes (4) and (5) occurred after the anomalies disappeared.

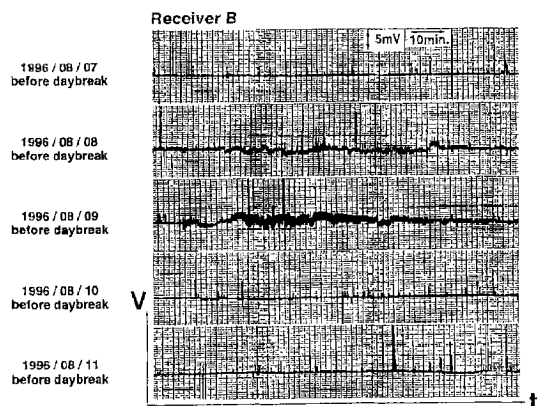


Fig. 8. Examples of CDS-anomalies. Typical parts of the charts recorded by the receiver B from 7 August 1996 to 11 August 1996 are shown. Weak anomalies began to appear on 7 August 1996 and combined anomalies were recorded on 9 August 1996. The anomaly became negligible on 10 August 1996 and an earthquake {4} occurred in the CD-sensitive region of the receiver B.

observed on the afternoon of 18 October 1996 by the receiver G and before daybreak on 19 October 1996 by the receiver H. Weak BTS-anomalies were also seen among the BT-anomalies.

An example of a CDS-anomaly is shown in Fig. 8, which was recorded by the receiver B in the period from 7 August 1996 to 11 August 1996. Two CDS-anomalies of opposite polarities are clearly observed on 9 August 1996. They are followed by continuous CDS-anomalies.

An apparent periodic oscillation of the baseline is shown in Fig. 9, which was obtained with receiver A from 12 to 14 July 1997. The period of the oscillation was about one minute. The oscillation can be regarded as a continuous repetition of CD-anomalies with short time constants.

The anomalies are easily smeared out by a direct radio wave delivery at the same frequency since they are weaker than meteor radio echoes and sporadic E. Therefore, if a radio station exists within the line of sight at the same radio frequency, it is necessary to limit the observation time during the pause of the broadcast of the radio station, which is often from midnight to daybreak. We carried out radio observations mainly during 0–6 a.m. Night observation has additional advantages because lesser number of aircraft fly over the observatory and lesser solar effects occur. However, we carried out 24-hour continuous observations when strong anomalies were observed.

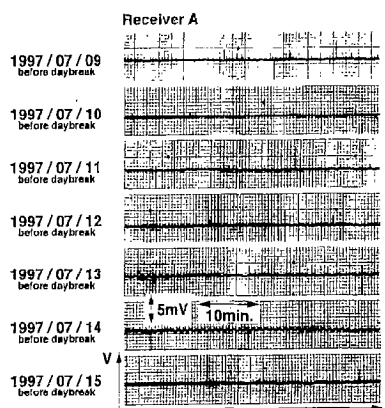


Fig. 9. An example of a CD-anomaly with short time constants. Typical parts of the charts recorded by the receiver A from 9 July 1997 to 15 July 1997 are shown. Small scale continuous CD-anomalies were observed on 12 and 14 July 1997. The period of the oscillatory signals was about one minute. On 13 July 1997, the oscillatory signal had a period of 2–3 minutes. The anomalies were too weak for forecasting earthquakes. The candidate earthquake is an undersea earthquake of M5.9 that occurred out of the CD-sensitive region of the receiver A on 15 July 1997.

Earthquake forecast

In this section, we describe a possible method of earthquake forecast based on the daily evolution of anomalies.

1. Anomaly strength We categorize the strength of CD- and CDS-anomalies into 7 ranks using the value of ξ combined with the number of appearances in a 6-hour observation which

is denoted by N_{6h} , as listed in Table 2. Rank-a denotes the CD-anomaly at the level of $\xi = 1$ appearing with $N_{6h} \geq 1$ or the CD-anomaly at the level of $\xi = 2$ appearing with $N_{6h} = 1-2$. Rank-b denotes the CD-anomaly at the level of $\xi = 2$ appearing with $N_{6h} = 3-4$ or the CD-anomaly at the level of $\xi = 3$ appearing with $N_{6h} = 1-2$. Rank-c denotes the CD-anomaly at the level of $\xi = 3$ appearing with $N_{6h} = 3-5$. Rank-d denotes the CD-anomaly at the level of $\xi = 4$ appearing with $N_{6h} \leq 4$. Rank-e denotes the continuously repeated CD-anomaly at the level of $\xi = 3$ or the CD-anomaly at the level of $\xi = 4$ appearing with $N_{6h} \geq 5$ or the CDS-anomaly appearing with $N_{6h} \geq 1$. Rank-f denotes the CDS-anomaly at the level of $\xi = 5$ appearing with $N_{6h} \geq 1$. Rank-g denotes the CDS-anomalies exceeding rank-f in ξ and N_{6h} .

Table 2. Ranks of the strengths of CD-anomalies and CD-components of CDS-anomalies categorized according to the significance ξ and the number of appearances in a 6-hour observation N_{6h} .

rank	CD-anomaly		CDS-anomaly	
	ξ	N_{6h}	ξ	N_{6h}
a	1	≥ 1	none	none
	2	1-2	none	none
b	2	3-4	none	none
	3	1-2	none	none
c	3	3-5	none	none
d	4	< 5	none	none
e	3	continuously repeated	none	none
	4	≥ 5	none	none
f	-	-	≥ 1	≥ 1
g	-	-	5	≥ 1
	-	-	exceeding rank-f	

The strength of BT- and BTS-anomalies is measured by the value of η .

2. Forecast of date Typical daily evolution of the anomaly strength is schematically illustrated in Fig. 10. The anomaly first appears at $t = t_1$, reaches the maximal value at $t = t_2$ and disappears at $t = t_3$ before earthquake occurs at $t = t_0$, where t denotes the time. The time difference $T_{FAP} = t_0 - t_1$ is referred to as the first appearance precedence. We refer to the periods of $t_1 \leq t \leq t_3$ and $t_3 \leq t \leq t_0$ as the period of anomaly appearance and the preseismic pause, respectively,

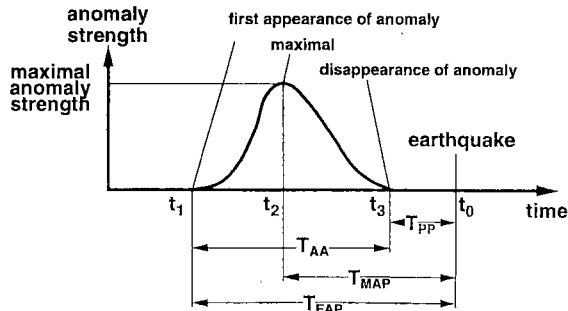


Fig. 10. Schematic illustration of the typical time evolution of the anomaly strength.

and we put $T_{AA} = t_2 - t_1$ and $T_{PP} = t_0 - t_3$. The time difference defined as $T_{MAP} = t_0 - t_2$ is referred to as the maximal-anomaly precedence.

In most cases, the first appearance precedence is in the range of $T_{FAP} = 4-8$ days. The maximal-anomaly precedence is about $T_{MAP} = 2-3$ days and the preseismic pause T_{PP} is about one day. An early warning can be made after the first appearance of the anomaly. The date of future earthquakes can be forecasted by observing the preseismic maximal of the anomaly strength and it can be refined after observing the preseismic pause. The anomaly strength at $t = t_2$, which is referred to as the maximal-anomaly strength, is used in the forecast of the magnitude of future earthquakes as discussed later.

In the case of earthquake swarm, both the period of anomaly appearance T_{AA} and the preseismic pause T_{PP} vary up to a few weeks which is much longer than the values mentioned above. The date forecast of earthquake swarm is limited by the variations in T_{AA} and T_{PP} and an ambiguity in maximal-anomaly identification since the daily evolution of the anomaly strength does not show a clear structure.

3. Forecast of focus location Each receiver is assumed to have a CD-sensitive region as shown in Fig. 11. The focus location can be forecasted according to the type of anomalies as schematically shown in Fig. 12.

When an earthquake focus is located below a CD-sensitive region, we refer to the corresponding receiver as the epicentral receiver. When the focus is located in the vicinities of a CD-sensitive region, the corresponding receiver is the vicinal receiver.

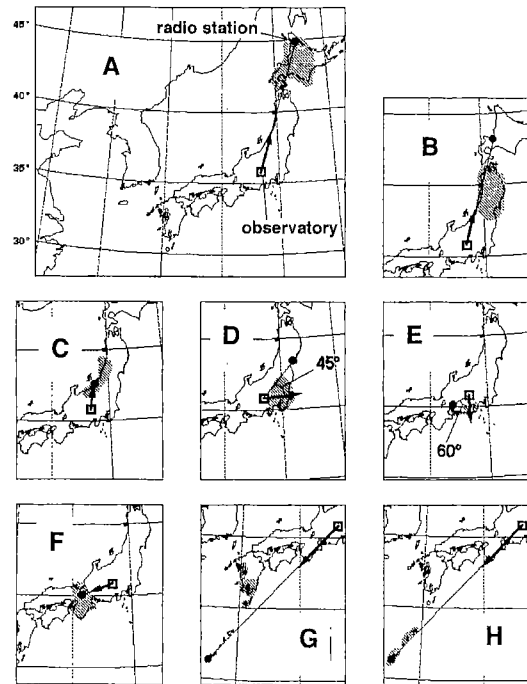


Fig. 11. CD-sensitive regions of receivers. The direction of the normal vector of the antenna plane is also shown in the figure. The offset angle θ is zero unless specified.

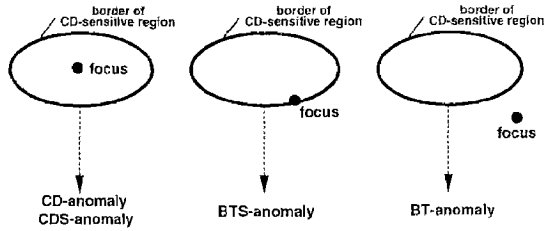


Fig. 12. Selectivity in types of anomalies according to the relationship between the focus location and the CD-sensitive region. Focus location of future earthquakes can be forecasted according to the distribution of CD-dominance and BT-dominance. CD- and CDS-anomalies imply that future earthquakes have their foci inside the corresponding CD-sensitive regions. BT-anomaly implies that the foci of future earthquakes are out of the corresponding CD-sensitive regions. If a BTS-anomaly is observed, the focus is close to the border of the corresponding CD-sensitive region.

CD-dominance is observed by epicentral receivers and BT-dominance is observed by vicinal receivers. In other words, CD-anomalies or CDS-anomalies are observed by receivers whose CD-sensitive regions contain the foci of future earthquakes. BT-anomalies are observed if the foci of future earthquakes is out of the CD-sensitive regions. BTS-anomalies are observed in the case where the foci of future earthquakes is located close to the border of a CD-sensitive region. Therefore, the focus location of future earthquakes can be forecasted from the distributions of CD-dominance and BT-dominance. The CD-sensitive regions in Fig. 11 were empirically determined so that they matched the above principles. The BT-component contained in the CDS-anomaly does not carry any information on the focus location, but provides information about the earthquake magnitude as described in the next subsection.

The focus location cannot be forecasted without the CD-component. The focus direction is forecasted with a lower reliability when only BT-anomalies are observed.

The time constant of the CD-component gives additional information. The time constant of the CD-component is about 5–10 minutes for underground earthquakes. The time constant becomes shorter as the foci of future earthquakes are located closer to the seashore and it becomes 1–2 minutes for undersea earthquakes. Therefore, the focus location forecast can be refined by an analysis of the time constant which has additional information of focus location in relation with distances from the sea.

4. Forecast of earthquake magnitude The maximal-anomaly strength can be related to the magnitude of future earthquakes regardless of focal depth. In other words, the focal depth cannot be forecasted by our method.

We introduce a parameter M_A which is referred to as anomaly magnitude. The parameter M_A is obtained from maximal-anomaly strength and the type of anomaly according to Table 3. The strength of the BT-component observed by vicinal receivers provides additional information for large earthquakes.

The value of M_A is the forecasted magnitude of future earth-

Table 3. Conversion of CD- and CDS-anomaly ranks into anomaly magnitude M_A . Strength of the BT-component observed by vicinal receivers is also taken into account in the conversion.

M_A	epicentral receiver	vicinal receiver
3	rank-a	none
4	rank-b	none
4.5	rank-c	none
5	rank-d	none
5.5	rank-e	$\eta = 1.5$ BT-anomaly
6	rank-f	$\eta = 2$ BT-anomaly
7	rank-g	$\eta \geq 2.5$ BT-anomaly

quakes as long as the earthquake has a single seismic activity. In the present paper, the correspondence between M_A and the magnitude of a future earthquake M is expressed as

$$M_A \leftrightarrow M. \quad (3)$$

A different conversion is applied in the case of multiple earthquakes. We put the magnitudes of individual earthquakes as M_i . We introduce a parameter L_i which is defined as

$$L_i = 10^{\alpha M_i - \beta}, \quad (4)$$

where $\alpha = 0.5$ and $\beta = 1.8$.⁵⁾ The value of M_A is related to the magnitude of future earthquake through the relation

$$M_A \leftrightarrow \frac{1}{\alpha} \left(\log_{10} \sum_{i=1}^n 10^{\alpha M_i - \beta} + \beta \right) = \bar{M}, \quad (5)$$

which implies that the magnitude of an individual earthquake M_i is summed over the parameter L_i . Equation (3) includes Eq. (5) as a case of $n = 1$.

Anomaly strength is attenuated for undersea earthquakes. The attenuation amounts to 0.5 and 1 in M_A for earthquakes whose foci are located in the close vicinities of the seashore and off shore within the border of the continental shelf, respectively. The value of M_A should be corrected for the case where the focus location of future earthquakes is forecasted undersea. Anomalies correlated with earthquakes whose foci are located at deep under sea positions are further attenuated and it is difficult to forecast the magnitude of these earthquakes.

5. Forecast examples Examples shown in the previous section can be interpreted as follows. The foci of future earthquakes for the case shown in Fig. 6 would be in the CD-sensitive region D because the CD-anomalies are observed by the receiver D. The focus would be underground because the time constant of the CD-anomalies is a few minutes. The anomaly strength attained its maximum on 28 July 1995 and disappeared by 30 July 1995, which implies that the earthquake would occur on 30 or 31 July 1995. The maximal anomaly had $\xi > 3$ without any BT-component. The anomaly magnitude was evaluated as $M_A = 5$. The candidate earthquake is the earthquake {1} in Table 4 ($M_{5.0}$) and occurred at 3:24 on 30 July 1995. The focus of the earthquake was at $N35^\circ 54' E140^\circ 36'$ in the CD-sensitive area of the receiver D.

Table 4. Earthquakes that occurred in CD-sensitive regions during the period of 24 July 1995 to 31 July 1997. M_A indicates the value after the correction of undersea attenuation. Earthquakes whose foci are located undersea deeper than the continental shelves are not listed in the table. (a) The M_A corresponding to {22} was not determined since corresponding receivers were disturbed by thunder clouds during the maximal period.

	date	epicenter and focal depth [km]	M	M_A
{1}	1995/07/30	N35°54' E140°36'	50	5.0
{2}	1996/02/07	N35°54' E136°36'	10	5.0
{3}	1996/03/06	N35°24' E138°54'	20	5.8
{4}	1996/08/11	N38°54' E140°36'	10	5.9
	1996/08/11	N38°54' E140°42'	10	5.4
	1996/08/11	N38°54' E140°42'	10	5.7
	1996/08/13	N38°48' E140°36'	10	5.0
{5}	1996/10/12	N36°06' E139°42'	90	4.9
{6}	1996/10/25	N35°30' E139°00'	30	4.9
{7}	1996/11/02	N34°18' E139°18'	10	5.0
{8}	1996/12/04	N37°24' E139°36'	150	5.5
{9}	1996/12/21	N38°06' E139°48'	40	5.5
{10}	1997/01/02	N35°24' E135°36'	360	5.3
{11}	1997/02/20	N37°24' E141°12'	90	5.4
{12}	1997/03/16	N34°54' E137°30'	40	5.6
{13}	1997/03/20	N36°54' E140°06'	70	4.8
{14}	1997/03/23	N36°00' E140°06'	70	4.9
{15}	1997/03/26	N32°00' E130°18'	20	6.2
	1997/03/26	N32°00' E130°18'	10	5.3
{16}	1997/04/03	N32°00' E130°18'	10	5.5
{17}	1997/04/09	N30°00' E130°24'	10	4.9
{18}	1997/05/12	N37°06' E141°18'	60	5.7
{19}	1997/05/13	N31°54' E130°18'	20	6.1
{20}	1997/05/18	N32°24' E130°36'	10	4.9
{21}	1997/05/22	N34°12' E139°12'	10	4.9
{22}	1997/06/05	N45°00' E141°18'	280	5.0
{23}	1997/06/15	N43°00' E144°12'	100	5.1
{24}	1997/07/09	N35°36' E140°06'	80	5.0

In the case of Fig. 7, the foci of future earthquakes would be in the close vicinity of CD-sensitive regions G and H because BT-anomalies are observed together with BTS-anomalies by the receivers G and H. The time constant of the BTS-anomalies is about a minute which suggests the possibility of undersea earthquake. The anomaly magnitudes of receiver G and H attained their maxima on 18 and 19 October 1996, respectively, which implied that an earthquake could occur one or two days after the maxima. The maximal-anomaly strength amounted to $\eta = 1.5$, which corresponds to $M_A = 5.5$. The value of $M_A = 6.5$ was obtained after adding the sea attenuation correction for an off shore case. Earthquakes {4} and {5} in Table 5 are the candidates corresponding to the BT-anomalies. Both these earthquakes occurred undersea and out of the CD-sensitive regions of receivers G and H.

In the case of Fig. 8, the foci of future earthquakes would be in the CD-sensitive region of receiver B because a CDS-anomaly was observed by the receiver B. The anomaly strength attained its maximum on 9 August 1996, which implied that the future earthquake would occur one or two days later. The maximum anomaly-strength corresponds to rank-f and $M_A = 6$. The focus location, the magnitude and the date of the earthquake {4} in Table 4 could be forecasted.

A small periodic oscillation with a period of one minute was observed by receiver A on 12 July 1997 as shown in Fig. 9. A small oscillation appeared with the period of a minute on 12

Table 5. Large earthquakes occurred out of CD-sensitive regions or at distant places in the direction of CD-sensitive regions. Correction of undersea attenuation is not included in M_A . (a) Maximal anomaly strength was not identified since the daily evolution did not show a clear maximal. The value of $M_A > 6$ was forecasted based on the average anomaly strength.

	date	epicenter	M	M_A
(1)	1996/01/01 17:05	N00°42' E119°54'	7.7	7
(2)	1996/02/03 20:14	Yunnan, China	6.9	6
(3)	1996/02/17 15:06	N00°00' E137°00'	8	(a)
(4)	1996/10/18	N30°36' E131°12'	6.2	5.5
(5)	1996/10/19	N31°48' E131°54'	7.0	6
(6)	1996/12/03	N31°48' E131°36'	6.3	5.5
(7)	1997/01/18	N28°48' E129°54'	6.0	6
(8)	1997/06/02	N26°54' E129°36'	5.7	5.5

July 1997. Successive CD-anomalies with longer periods were observed on 13 July 1997. On 14 July 1997, the oscillation with a period of one minute was again observed and subsequently disappeared on 15 July 1997. An undersea earthquake was expected because the anomalies were explained as successive CD-anomalies with shorter time constants of the order of a minute. However, the anomalies were too weak to forecast the magnitude and the focus location of future earthquakes. The candidate earthquake is an undersea earthquake M5.9 and occurred at 1:09 hours on 15 July 1997. The focus was at N43°12' E146°30' and the focal depth was 40 km. The focus location was out of the CD-sensitive region A.

6. Forecast summary The earthquake forecasts are visualized in Fig. 13. Large anomalies with $M_A \geq 5$ which were observed during the observation period are shown together with the earthquakes and occurred inside or in the vicinity of the CD-sensitive regions. The observed anomalies are classified into four groups in the figure: CD-anomaly, CDS-anomaly, BT- and BTS-anomalies and exceptional anomaly. The closed bar shows the period of appearance of the CDS-anomaly, hatched bar the CD-anomaly, open bar the BT- and BTS-anomalies, and the gray bar the exceptional anomaly. Earthquakes are shown in the figure as circles. Closed circle shows the day on which an earthquake listed in Table 4 occurred inside a CD-sensitive region. A gray circle indicates the day on which a large earthquake occurred out of the CD-sensitive regions, mostly undersea or at distant places in the direction towards a CD-sensitive region. The period during which an earthquake swarm took place is marked with open circles.

Figure 13 shows that the anomalies were observed ahead of earthquakes. In addition, the earthquake magnitude is well correlated with the forecasted anomaly magnitude listed in Table 4.

Smaller anomalies also appeared before smaller earthquakes. Our observation is capable of detecting anomalies corresponding to earthquakes of $M \geq 3$. However, they are not analyzed in this paper since M3-class earthquakes occur too frequently to identify the correspondence between anomalies and the earthquakes.

Our results can be summarized as follows. First, the first anomaly precedence is about $T_{FAP} = 4-8$ days and the pre-seismic pause is $T_{PP} \sim 1$ day. It is possible to forecast the

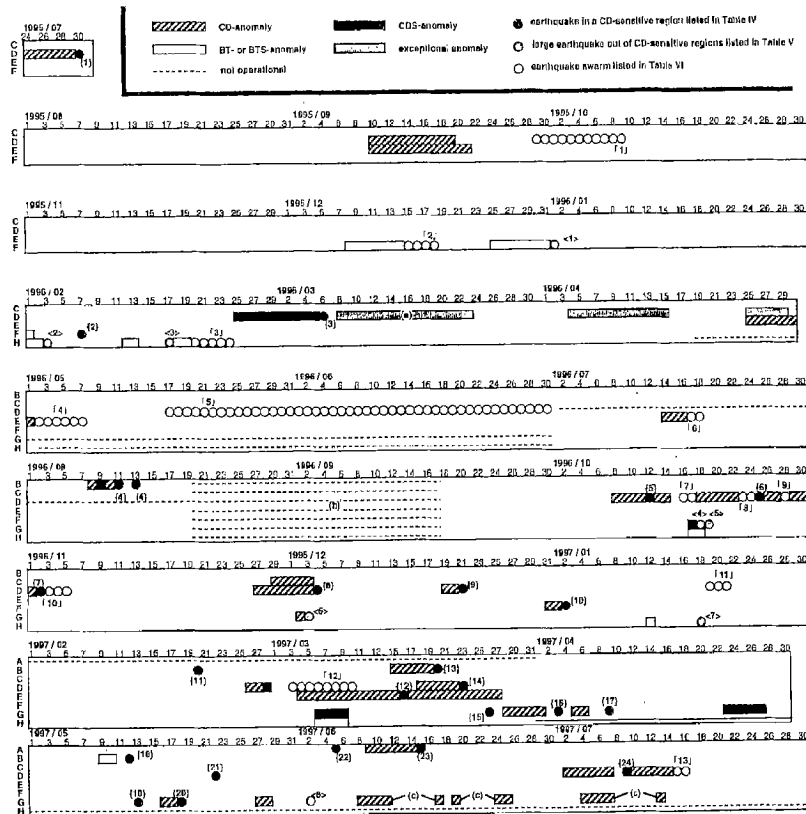


Fig. 13. Correlation between anomalies and earthquakes. Anomalies with $M_A \geq 5$ which were observed during the observation period are shown together with earthquakes that occurred inside or in the vicinities of the CD-sensitive regions. Closed bar shows the period when the CDS-anomaly was observed, hatched bar the CD-anomaly, open bar the BT- and BTS-anomalies, and gray bar the exceptional anomaly. Earthquakes are shown in the figure as circles. Closed circle indicates the day on which an earthquake listed in Table 4 occurred inside a CD-sensitive region. A gray circle indicates the day on which a large earthquake occurred out of CD-sensitive regions. The period during which an earthquake swarm took place is marked with open circles. The dotted line shows that data are unavailable since the receiver was not operational. (a) Exceptional anomalies appeared on 8 March 1996 on the charts of the receiver D. The baseline was completely flat in the anomalies without the usual baseline fluctuation due to noises, signals of meteor radio echoes and aircraft. (b) Observation data are not useful because of the interference among receiver antennas. The antenna location and direction were rearranged to avoid the interference. (c) Weak anomalies were occasionally observed from June up to the middle of July 1997 by the receiver G. These are regarded as effects related to small aftershocks of the earthquake {20} in the CD-sensitive region of the receiver G and small earthquakes in the CD-sensitive region of the receiver H.

date of the earthquake with an uncertainty of a few days except for the case of an earthquake swarm which shows longer T_{AA} and T_{PP} . The behaviors of T_{AA} and T_{PP} have not been studied in detail so as to be applied to the forecast of date.

Second, in most cases, the maximal-anomaly precedence is equal to $T_{MAP} = 2-4$ days and the anomaly magnitude coincides with the earthquake magnitude with a forecast error of about ± 0.8 . The anomaly magnitude is correlated only with the earthquake magnitude and is independent of the focal depth.

Third, the focus location can be forecasted from the distribution of the type of dominant components in anomalies. Future earthquakes are expected to occur in the CD-sensitive region of the receiver which has recorded CD-anomalies or CDS-anomalies. If a receiver records BT-anomalies, future earthquakes are expected to occur out of its CD-sensitive region. BTS-anomalies imply that future earthquakes are expected to occur on the border of the CD-sensitive region. However,

the locations of multiple earthquakes occurring in one CD-sensitive region in a short time period cannot be forecasted individually.

Finally, the CD-sensitive region is limited by the attenuation effect of sea water. Earthquakes whose foci are located deeper than the continental shelves are almost undetectable unless the earthquake magnitude is large enough to overcome the attenuation of more than 1 in magnitude.

Although the radio stations g and h are located almost at the same position, corresponding CD-sensitive regions G and H are entirely different. Similar situation is also seen for the case of A and B. The major difference between receivers G and H and between A and B is the radio power of the corresponding radio stations. This suggests that the selectivity is caused according to the difference in the radio power. We parameterize the distance to the center of the CD-sensitive region from the observatory L as $(L/r - 1)^2 = P/P_0$, where P is the power of the FM radio station and r is the distance

to the radio station. The parameter P_0 is estimated to be $P_0 = 27$ kW. The radius of the CD-sensitive region ρ is about 130 km. The value of ρ seems to increase as L increases.

Exceptional anomalies appeared on 8 March 1996 on the charts of the receiver D. Baseline was completely flat in the anomalies without the usual baseline fluctuations due to noises, signals of meteor radio echoes and aircraft. The anomalies continued intermittently up to the end of April 1996 without any apparent earthquakes. Later, we learned that an imperceptible earthquake swarm had started from the middle of May 1996 and lasted up to the end of June 1996 in the region of N35°18'-N35°30' E140°18'-E140°42', which is listed as Ref. 5 in Table 6. The total magnitude amounted M6.3.⁶⁾ The imperceptible earthquake swarm is presumed as the corresponding earthquake.

Table 6. Earthquake swarms occurred in the CD-sensitive regions during the observation period. \bar{M} is the sum of the magnitudes of individual earthquakes through L according to Eq. (5), to which the value of M_A corresponds. n is the number of perceptible earthquakes involved in each item. All earthquake swarms listed in this table occurred undersea closer to seashore than near the border of continental shelves. M_A indicates the value after the correction of undersea attenuation. (a) The anomaly strength was assumed to be $M_A = 5$ at the moment of forecast because we did not know how to treat the daily evolution with long T_{AA} and T_{PP} at that moment. The value listed in the table is the result of reanalysis of the past data. (b) Calculated from only 3 earthquakes that occurred from 16 to 18 December 1995 because the seismograph was not available. The real value of \bar{M} can be larger than 5. 1. (c) Imperceptible earthquake swarm. This is regarded as being related to the exceptional anomalies observed by the receiver D. The value of \bar{M} is taken from Ref. 7, and not calculated from Eq. (5).

	date	epicenter	\bar{M}	n	M_A
[1]	1995/09/29-10/09	N35°00' E139°06'	7.4	59	6 ^(a)
[2]	1995/12/15-12/18	N29°18' E129°12'	5.1 ^(b)	3	5.5
[3]	1996/02/20-02/24	N29°12' E129°12'	5.8	11	5.5
[4]	1996/05/02-05/07	N34°18' E139°12'	5.7	8	5.5
[5]	1996/05/17-06/30	N35°24' E140°30'	6.5 ^(c)	-	(c)
[6]	1996/07/17-07/18	N34°24' E139°12'	5.9	8	5.5
[7]	1996/10/16-10/17	N35°00' E139°06'	5.5	10	5
[8]	1996/10/23-10/25	N34°12' E139°12'	5.9	20	5.5
[9]	1996/10/28	N34°18' E139°12'	6.0	14	5.5
[10]	1996/11/02-11/05	N34°18' E139°12'	5.2	12	5
[11]	1997/01/19-01/21	N34°30' E139°12'	5.8	14	4.5
[12]	1997/03/03-03/10	N35°00' E139°06'	7.4	42	6
[13]	1997/07/15-07/16	N34°42' E139°18'	4.7	11	5.5

Discussion

We propose a model to explain the mechanism of the correlation between earthquakes and anomalies in radio observations in the VHF band.

The first assumption is that the anomalies in the radio observation are caused by the time variation of the intensity of radio waves scattered in the ionosphere. It seems natural to assume that the radio waves are delivered by scattering because the radio programs are not demodulated with the anomalies, while they are demodulated with radio echoes due to meteors and sporadic E.

The second assumption is that the time variation of the radio

wave scattering is enhanced above the foci of future earthquakes. A CD-anomaly can be explained as a result of a real charge and discharge process of a capacitor formed with the earth's surface and the ionosphere. During the preseismic period, electric charge is accumulated on the earth's surface due to generation of microcracks in underground rocks. After the electric charge induces a change in electron density in the ionosphere, it is discharged through the atmosphere. Similarly, a BT-anomaly may be the result of the backward scattering of radio waves from the electron density change of a large volume. In addition, the fact that the anomaly strength is attenuated for undersea earthquakes can be explained as a faster discharge due to the electric conductance of sea water. This is consistent with the fact that the anomaly magnitude has a simple relation with the earthquake magnitude and not with the focal depth.

For a more quantitative conversion between anomaly strength and M_A , we measured the anomaly magnitude as the number of black dots of digitally scanned images of the charts. The numbers of black dots of $M_A = 5$ and $M_A = 6$ are 1.9 and 2.8 times larger respectively than that of $M_A = 4$ after extracting meteor radio echoes. This suggests the possibility of numerical formulation of the anomaly strength using a simple integral of time variation of the baseline. However, it is difficult to analyze the entire data more quantitatively since data were recorded on chart recorders. A more quantitative analysis is in progress by recording the voltage of the center tuning meters using analog to digital converters in collaboration with The Institute of Physical and Chemical Research.⁷⁾

In our method, the choice of the CD-sensitive region is limited since ordinary broadcasting radio waves are observed from only one observatory. Simultaneous observation from different observatories will contribute towards improvement in the study of the correlation between anomalies and earthquakes. The interference in observations due to nearby radio stations at the same radio frequency can be avoided by reserving a radio channel, which will enable us to carry out a 24-hour continuous monitoring. Further study of the characteristics of delivered radio waves is necessary to identify the mechanism behind the correlation between anomalies and earthquakes.

The authors are grateful to Drs. T. Ebisuzaki, H. M. Shimizu, T. Oku and K. Sunouchi of The Institute of Physical and Chemical Research for their support and discussions. We thank Mr. H. Tanbo of The Yatsugatake South Base Observatory for his help and suggestions in the early stage of this research. We also thank Drs. J. Watanabe and R. Kawabe of The National Astronomical Observatory for their suggestions.

References

- 1) J. S. Hey and G. S. Stewart: Proc. Phys. Soc. **59**, 858 (1947).
- 2) Y. Kushida: Parity Vol. 10, No. 10, p. 79 (1995) (in Japanese).
- 3) K. Saito and T. Nakagawa: *Ryusei* (Meteor) (Koseisha-Koseikaku, Tokyo, 1984) p. 140 (in Japanese).
- 4) Weathernews Inc. URL: <http://www.wni.co.jp/>.
- 5) The parameter L indicates the diameter of the aftershock region measured in kilometers. See T. Utsu: *Jishingaku* (Seismology) (Kyoritsu Publishing, Tokyo, 1984) 2nd ed. (in Japanese).
- 6) T. Sagiya: Eos Transact. Am. Geophys. Union **78**, S214 S31C-7 (1997).
- 7) T. Oku et al.: to be published.